Published in final edited form as:
Angew Chem Int Ed Engl. 2011 April 4; 50(15): 3430–3434. doi:10.1002/anie.201007461.

Design of Highly Emissive Polymer Dot Bioconjugates for *in vivo* Tumor Targeting**

Changfeng Wu,
Department of Chemistry, University of Washington, Seattle, WA 98195 (USA)

Stacey J. Hansen,
Clinical Research Division, Fred Hutchinson Cancer Research Centre, Seattle, WA 98109 (USA)

Prof. Qiong Hou,
School of Chemistry and Environment, South China Normal University, Guangzhou, Guangdong 510631 (China)

Jiangbo Yu,
Department of Chemistry, Clemson University, Clemson SC, 29634 (USA)

Maxwell Zeigler,
Department of Chemistry, University of Washington, Seattle, WA 98195 (USA)

Yuhui Jin,
Department of Chemistry, University of Washington, Seattle, WA 98195 (USA)

Daniel R. Burnham,
Department of Chemistry, University of Washington, Seattle, WA 98195 (USA)

Prof. Jason D. McNeill,
Department of Chemistry, Clemson University, Clemson SC, 29634 (USA)

Prof. James M. Olson, and
Clinical Research Division, Fred Hutchinson Cancer Research Centre, Seattle, WA 98109 (USA)

Prof. Daniel T. Chiu*
Department of Chemistry, University of Washington, Seattle, WA 98195 (USA)

Nanoparticle-based diagnostic and therapeutic agents have attracted considerable interest because of their potential for clinical oncology and other biomedical research.[1] Versatile nanostructures have been demonstrated for *in vivo* applications, such as lipid and polymeric nanocapsules for drug delivery,[2] iron oxide nanoparticles for magnetic resonance imaging,[3] gold nanoparticles for X-ray computed tomography,[4] and quantum dots (Qdots) for fluorescence imaging.[5] Qdots represent one of the exciting nanotechnologies translated to biology in the past decade. The size-tunable luminescence makes them appealing as multicolor fluorophores for biological labelling, imaging, and sensing.[6,7] For *in vivo* applications, however, the intrinsic toxicity of Qdots is of critical concern,[8] which may impede their final clinical translation. Therefore, the design of bright probes with biologically benign materials is highly desirable for many *in vivo* clinical applications.

**This work was supported by the National Institutes of Heath (CA147837 and NS062725 to D.T.C.; CA135491 and CA112350-03 to J.M.O.; GM 081040 to J.D.M.). We acknowledge support from the Keck Imaging Center, the Center of Nanotechnology at the University of Washington, and the Seattle Children's Research Institute Brain Tumor Endowment.

*Fax: (+1) 206-685-8665, chiu@chem.washington.edu.

Supporting information for this article is available on the WWW under http://www.angewandte.org or from the author.

Semiconducting polymer dots (Pdots) represent a new class of fluorescent probes because of their high brightness and non-toxic feature.[9–15] Although still at the early stage of development, Pdots are attracting intense interest.[12,13] Researchers have developed various methods to improve the versatility and functions of Pdots for biomedical studies, such as tuning the emission color,[16] exploring new preparation methods,[17] engineering the particle surface,[18] doping functional sensing molecules,[19,20] encapsulating magnetic materials,[21] and mapping sentinel lymph node as a first *in vivo* study.[22] We have recently developed a general method to form Pdot-bioconjugates, and demonstrated their applications in specific cellular targeting and bioorthogonal labelling.[23,24]

Despite the various efforts, there are still several challenges associated with Pdots as *in vivo* probes. First, the fluorescence brightness of Pdots in the red and near infrared (NIR) is generally limited by their low quantum yields. Second, it is unclear whether Pdot-based probes can be specifically delivered to diseased tissues *in vivo*. Here we show highly fluorescent Pdots consisting of optimally tailored semiconducting polymer blends for *in vivo* tumor targeting. The polymer-blend dots (PBdots) exhibited large absorptivity (3.0×10^7 $cm^{-1}M^{-1}$ at 488 nm) and efficient deep-red emission (quantum yield = 0.56), making them ~15 times brighter than the commercial 655 nm-emitting Qdots. We covalently conjugated the PBdots to a tumor-specific peptide ligand, and demonstrated their specific targeting to malignant brain tumors in a genetically engineered mouse model.

Various semiconducting polymers can be used to prepare small Pdots as fluorescent labels.[11] Polyfluorenes (PF) and their derivatives in particular exhibit great flexibility for designing fluorescent probes as shown by the significant success made so far in tuning their emission color from blue to deep-red region by introducing narrow-band-gap monomers into the polymer backbone.[25,26] However, the fluorescence quantum yield, particularly in the deep-red region, precipitously drops as the concentration of narrow-band-gap monomers is increased. As a trade-off, therefore, only a small amount of narrow-band-gap monomers can be incorporated into the PF copolymer so as to maintain a high fluorescence quantum yield. This constraint results in deep-red emitting Pdots that only have significant absorption feature in the ultraviolet (UV) region (Supporting Information, Figure S1), which is a severe drawback for *in vivo* applications. This communication describes our strategy to overcome this issue by designing polymer blended Pdots, which have both excellent absorption cross-section in the visible range and high quantum yield in deep-red emission.

Based on the efficient intra-particle energy transfer in Pdots,[19,27] we designed nanoparticles consisting of donor-acceptor polymer blends to overcome the UV-absorption limitation. The polymer-blend dots (PBdots) were prepared by using a visible-light-harvesting polymer (PFBT) as the donor and an efficient deep-red emitting polymer (PF-DBT5) as the acceptor (Figure 1a). Because the donor and acceptor polymers were closely packed into single dots, intra-particle energy transfer resulted in complete quenching of the PFBT donor and intense fluorescence from the acceptor polymer alone (Supporting Information, Figure S2a). At a blending ratio of 0.6 (PF-DBT5 to PFBT in weight), the PBdots exhibited a broad visible absorption band extending to 600 nm and an efficient 650 nm emission with a quantum yield of 0.56 (Figure 1b, Supporting Information, Figure S2b). This value represents the highest among various Pdots reported thus far. The blending strategy was also successfully applied to other polymer donor-acceptor systems consisting of light-harvesting polymer PFPV and different red- emitting polymers (Supporting Information, Figure S3), indicating its general applicability for tuning Pdot properties.

Chlorotoxin (CTX), a 36-amino acid peptide, was selected as a tumor-targeting ligand because it has a strong affinity for tumors of neuroectodermal origin.[28] We functionalized the PBdots using an amphiphilic polymer, poly(styrene-co-maleic anhydride) (PSMA), to

generate surface carboxyl groups (Figure 1a).[24] The carboxyl groups enabled CTX conjugation by the standard carbodiimide chemistry.[29] Polyethylene glycol (PEG) was also conjugated to reduce protein adsorption, limit immune recognition, and thereby increase the nanoparticle serum half-life *in vivo*. As a separate control, streptavidin was used to verify the conjugation strategy by specific cellular labelling. Transmission electron microscopy (TEM) indicated an average particle diameter of ~15 nm for the functionalized PBdots (Figure 1c). After conjugation to different molecules (PEG, CTX, and streptavidin), gel electrophoresis showed shifted migration bands of the PBdot-conjugates in a 0.7% agarose gel due to the changes in surface charge and particle size (Figure 1d), thus indicating successful carboxyl functionalization and surface bioconjugation.

We performed single-particle imaging to compare the brightness of the PBdot against that of a Qdot that emits at 655 nm (the brightest commercially available Qdot probe from Invitrogen). We used a 488-nm laser excitation power so that Qdot 655 can be reasonably detected (Figure 2a). But under identical acquisition and laser conditions, the majority of PBdots actually saturated the detector. This prominent difference is attributed to the high molar extinction coefficient of PBdots (~3.0×10^7 $cm^{-1}M^{-1}$ at 488 nm for nanoparticles of ~15 nm diameter). To avoid detector saturation, we placed a neutral density filter (optical density of 1, which blocks 90% of the emitted fluorescence) together with the emission filter to obtain single-particle fluorescence images of PBdots (Figure 2b). Fluorescence images of thousands of individual particles were collected and their fluorescence intensities were back-calculated according to the attenuation factor. Fluorescence intensity distribution indicated that PBdot were ~15 times brighter than Qdot 655 (Figure 2c), consistent with the brightness comparison based on the bulk spectra analysis. Fluorescence lifetime of PBdots was determined to be 3.5 ns with a time-correlated single-photon counting instrument (TCSPC) (Supporting Information, Figure S4).

We investigated the binding selectivity of PBdot-bioconjugates. PBdot-streptavidin probes were used to label a specific cellular target, EpCAM, an epithelial cell-surface marker currently used for the detection of circulating tumor cells. Figure 2d shows that the PBdot-streptavidin successfully labeled EpCAM receptors on the surface of live MCF-7 human breast cancer cells after the cells were incubated sequentially with a primary anti-EpCAM antibody and a biotinylated goat anti-mouse IgG secondary antibody. When the cells were incubated with primary antibody and PBdot-streptavidin in the absence of the secondary antibody, fluorescence was not observed on the cell surface (Figure 2e), indicating that the PBdot-bioconjugates were highly specific for the target. The photostability of PBdots was further compared with that of a small-molecule dye commonly used in cellular labeling. We monitored the fluorescence intensity changes of both the PBdot labelling of the cell surface and the Hoechst nuclear stain under continuous laser scanning for 20 minutes on a confocal microscope (Supporting Information, Figure S5). Photobleaching curves extracted from the fluorescence images indicate the PBdots were much more photostable than the organic dye (Figure 2f). The PBdots are also stable in serum for weeks, without aggregation and decrease in fluorescence intensity.

Delivering imaging probes to brain tumors represents one of the most challenging *in vivo* tasks because of the exclusive blood-brain barrier and the complex dependence on the probe size and surface properties.[3] We evaluated the capability of the PBdot-CTX conjugate to traverse the blood-brain barrier and specifically target a tumor in a transgenic mouse model, ND2:SmoA1. We chose this mouse model because it closely resembles human medulloblastoma, the most common, malignant, childhood brain tumor.[30] The ND2:SmoA1 tumor arises spontaneously in the cerebellum and maintains an intact blood-brain barrier.[28] A detailed description of molecular targets of CTX for tumor targeting is provided in Supporting Information. PBdot probes were injected into each animal, either

symptomatic ND2:SmoA1 or wild-type (as a control), through the tail vein. The PBdot probes were either targeting PBdot-CTX or nontargeting PBdot-PEG (as a probe control). The ability of PBdot probes to specifically target tumors was assessed by biophotonic imaging.

Figure 3a shows typical *ex vivo* biophotonic images of mouse brains at 72 hours post-injection. Preferential accumulation of the PBdot-CTX in ND2:SmoA1 tumors was evident by the strong fluorescence signal observed only in the brain tumor regions of the mice that received the targeting probes (the right image in the middle row in Figure 3a). In contrast, significantly lower levels of fluorescence were detected in the tumors of mice that received the non-targeting PBdot-PEG probes (the right image in the top row in Figure 3a), indicating the specific tumor targeting of PBdots due to the conjugation of CTX ligand. The ND2:SmoA1 mouse that did not receive an injection showed a similar fluorescence signal as those that received the non-targeting PBdot probes. Specific targeting of the PBdot-CTX probes to ND2:SmoA1 tumors was further counter-illustrated with wild-type mice (bearing no tumors) injected with the PBdot probes, which showed no PBdot accumulation in the healthy brains (Figure 3a, left). Comparable imaging results were obtained for ND2:SmoA1 and wild-type animals 24 hours after they were injected with PBdot probes (Supporting Information, Figure S6), which suggest the accumulation of PBdot-CTX nanoprobe in the brain tumor was complete within 24 hours, and the signal intensity remained steady for the remaining 48 hours of the 72-hour analysis.

Quantitative evaluation of the PBdot accumulation further confirmed the specific tumor targeting of the PBdot-CTX conjugates. When the targeting PBdot-CTX probes were injected, the fluorescence intensity in the brain regions of ND2:SmoA1 relative to wild-type animals showed a 2.3±0.2-fold increase (mean±s.d., $P<0.01$), compared with a minimal change (1.2±0.1 fold, $P>0.05$) by using non-targeting PBdot-PEG probes (Figure 3b). This signal increase was comparable to the NIR-emitting CTX:Cy5.5 bioconjugate.[28] For a given ND2:SmoA1 or wild-type animal, fluorescence intensity in the frontal lobe (healthy tissue) of the cerebral hemisphere and the cerebellum (tumor containing tissue) in the same animal was also analyzed (Figure 3b). Again, significant signal increase (2.2±0.3 fold, $P<0.01$) in the cerebellum versus the frontal lobe was only observed in the ND2:SmoA1 mice that received targeting PBdot-CTX probes, whereas a minimal change (1.1±0.2 fold, $P>0.05$) was seen for the ND2:SmoA1 mice that received non-targeting PBdot-PEG probes. No apparent signal difference between the cerebellum and the frontal lobe was observed in wild-type animals regardless of whether targeting or non-targeting probes were injected. To determine the accuracy of tumor regions as highlighted by PBdot-CTX, histological analysis was performed on the excised brains of the mice after biophotonic imaging. The dark purple regions in the H&E-stained cerebellum of the ND2:SmoA1 mice clearly outline the tumors as compared to the wild-type mouse (Figure 3c). The histological analysis correlated well with the biophotonic images, confirming the selective accumulation of the targeting PBdot-CTX probes in the malignant brain tumors.

The nanoparticle clearance and biodistribution are closely dependent on particle size.[31,32] For nanoparticles that have a hydrodynamic diameter of 10–20 nm, the only major route of excretion from the animal body is through the liver into bile and feces.[32] There was no observable fluorescence signal in blood at 72 hours post-injection from the PBdot-CTX probes (Supporting Information, Figure S7). We investigated the distribution profiles in the main clearance organs including liver, spleen, and kidney by *ex vivo* fluorescence signal quantification of the resected tissues (Figure 3d). The biodistributions in the wild-type animals that received the PBdot-CTX injection and the ND2:SmoA1 mice that were not injected were also analyzed (Figure 3d). As expected based on particle size,[32] the PBdot-CTX exhibited dominant uptake in liver, significantly lower signal in spleen, and nearly no

distribution in kidney for both wild-type and ND2:SmoA1 mice (Figure 3e). This distribution profile is comparable to those reported for inorganic iron oxide nanoparticles and quantum dots of similar particle size.[3,32]

In summary, we designed a polymer-blend nanodot system consisting of donor-acceptor polymers for *in vivo* tumor targeting. The large absorptivity and high fluorescence quantum yield make the PBdots ~15 times brighter than the 655 nm-emitting Qdots. To our knowledge, it represents the brightest nanoprobe at present among various fluorescent nanoparticles of similar size (~15 nm). We covalently conjugated the PBdots to a peptide ligand CTX, and demonstrated their specific targeting to malignant brain tumors by biophotonic imaging, biodistribution and histological analyses. This study provides a new type of nanoparticle platform that holds promise for clinical cancer diagnostics.

Experimental Section

Functionalized PBdots in aqueous solution were prepared by using a modified nano-precipitation method. Surface bioconjugation was performed by utilizing the EDC-catalyzed reaction between carboxyl PBdots and the respective amine-containing biomolecules.

All mouse studies were conducted with procedures approved by the Institutional Animal Care and Use Committee at Fred Hutchinson Cancer Research Center. Transgenic ND2:SmoA1 mice were generated on a C57BL/6 background. Non-genetically altered C57BL/6 mice were used as wild-type controls. ND2:SmoA1 mice or C57BL/6 wild type controls were injected with 50 μl of a 1 μM solution of PBdot-CTX or PBdot-PEG through the tail vein. One or three days after injection the mice were euthanized using CO_2 inhalation and their brains removed for *ex vivo* fluorescent imaging. *Ex vivo* images were obtained using the Xenogen/Caliper Spectrum Imaging System. For biodistribution, C57BL/6 wild type and ND2:SmoA1 mice were injected with 50 μl of 1 μM PBdot-CTX through the tail vein. Three days after injection, the mice were euthanized, blood, liver, kidney, and spleen were removed and analyzed using *ex vivo* imaging techniques as described above.

A full description of the materials, methods, and additional Figures S1–S7 are provided in the Supporting Information.

Supplementary Material

Refer to Web version on PubMed Central for supplementary material.

References

1. Ferrari M. Nat. Rev. Cancer. 2005; 5:161. [PubMed: 15738981]
2. Sengupta S, Eavarone D, Capila I, Zhao GL, Watson N, Kiziltepe T, Sasisekharan R. Nature. 2005; 436:568. [PubMed: 16049491]
3. Veiseh O, Sun C, Fang C, Bhattarai N, Gunn J, Kievit F, Du K, Pullar B, Lee D, Ellenbogen RG, Olson J, Zhang MQ. Cancer Res. 2009; 69:6200. [PubMed: 19638572]
4. Popovtzer R, Agrawal A, Kotov NA, Popovtzer A, Balter J, Carey TE, Kopelman R. Nano Lett. 2008; 8:4593. [PubMed: 19367807]
5. Gao X, Cui Y, Levenson RM, Chung LWK, Nie S. Nat. Biotechnol. 2004; 22:969. [PubMed: 15258594]
6. Medintz IL, Uyeda HT, Goldman ER, Mattoussi H. Nat. Mater. 2005; 4:435. [PubMed: 15928695]
7. Michalet X, Pinaud FF, Bentolila LA, Tsay JM, Doose S, Li JJ, Sundaresan G, Wu AM, Gambhir SS, Weiss S. Science. 2005; 307:538. [PubMed: 15681376]
8. Derfus AM, Chan WCW, Bhatia SN. Nano Lett. 2004; 4:11.
9. Wu C, Szymanski C, McNeill J. Langmuir. 2006; 22:2956. [PubMed: 16548540]

10. Wu C, Szymanski C, Cain Z, McNeill J. J. Am. Chem. Soc. 2007; 129:12904. [PubMed: 17918941]
11. Wu C, Bull B, Szymanski C, Christensen K, McNeill J. ACS Nano. 2008; 2:2415–2423. [PubMed: 19206410]
12. Pecher J, Mecking S. Chem. Rev. 2010; 110:6260. [PubMed: 20684570]
13. Kaeser A, Schenning APHJ. Adv. Mater. 2010; 22:2985. [PubMed: 20535737]
14. Moon JH, McDaniel W, MacLean P, Hancock LE. Angew. Chem. Int. Ed. 2007; 46:8223.
15. Pu KY, Li K, Shi JB, Liu B. Chem. Mater. 2009; 21:3816.
16. Abbel R, van der Weegen R, Meijer EW, Schenning APHJ. Chem. Commun. 2009:1697.
17. Baier MC, Huber J, Mecking S. J. Am. Chem. Soc. 2009; 131:14267–14273. [PubMed: 19764722]
18. Howes P, Green M, Levitt J, Suhling K, Hughes M. J. Am. Chem. Soc. 2010; 132:3989–3996. [PubMed: 20175539]
19. Wu C, Zheng Y, Szymanski C, McNeill J. J. Phys. Chem. C. 2008; 112:1772.
20. Wu C, Bull B, Szymanski C, Christensen K, McNeill J. Angew. Chem. Int. Ed. 2009; 48:2741–2745.
21. Howes P, Green M, Bowers A, Parker D, Varma G, Kallumadil M, Hughes M, Warley A, Brain A, Botnar R. J. Am. Chem. Soc. 2010; 132:9833. [PubMed: 20572665]
22. Kim S, Lim CK, Na J, Lee YD, Kim K, Choi K, Leary JF, Kwon IC. Chem. Commun. 2010; 46:1617.
23. Wu C, Schneider T, Zeigler M, Yu J, Schiro P, Burnham D, McNeill JD, Chiu DT. J. Am. Chem. Soc. 2010; 132:15410. [PubMed: 20929226]
24. Wu C, Jin Y, Schneider T, Burnham DR, Smith PB, Chiu DT. Angew. Chem. Int. Ed. 2010 In Press.
25. Hou Q, Zhou QM, Zhang Y, Yang W, Yang RQ, Cao Y. Macromol. 2004; 37:6299.
26. Yang RQ, Tian RY, Yan JG, Zhang Y, Yang J, Hou Q, Yang W, Zhang C, Cao Y. Macromol. 2005; 38:244.
27. Wu C, Peng H, Jiang Y, McNeill J. J. Phys. Chem. B. 2006; 110:14148. [PubMed: 16854113]
28. Veiseh M, Gabikian P, Bahrami SB, Veiseh O, Zhang M, Hackman RC, Ravanpay AC, Stroud MR, Kusuma Y, Hansen SJ, Kwok D, Munoz NM, Sze RW, Grady WM, Greenberg NM, Ellenbogen RG, Olson JM. Cancer Res. 2007; 67:6882. [PubMed: 17638899]
29. Hermanson, GT. Bioconjugate Techniques. 2nd ed.. San Diego: Academic Press; 2008.
30. Hatton BA, Villavicencio EH, Tsuchiya KD, Pritchard JI, Ditzler S, Ptfflar B, Hansen S, Knoblaugh SE, Lee D, Eberhart CG, Hallahan AR, Olson JM. Cancer Res. 2008; 68:1768. [PubMed: 18339857]
31. Choi HS, Liu WH, Liu FB, Nasr K, Misra P, Bawendi MG, Frangioni JV. Nat. Nanotechnol. 2010; 5:42. [PubMed: 19893516]
32. Choi HS, Liu W, Misra P, Tanaka E, Zimmer JP, Ipe BI, Bawendi MG, Frangioni JV. Nat. Biotechnol. 2007; 25:1165. [PubMed: 17891134]

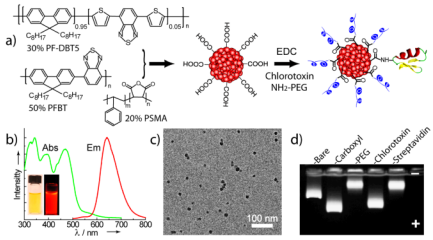

Figure 1.

a) PBdot functionalization and CTX conjugation. A light-harvesting polymer PFBT, a red-emitting polymer PF-DBT5, and a functional polymer PSMA were co-condensed to form highly fluorescent PBdots with surface carboxyl groups. The carboxyl groups enabled further surface conjugation to a tumor-specific peptide ligand CTX (depicted as red-green-yellow string). b) Absorption and emission spectra of PBdot. The inset shows photographs of aqueous PBdot solution under room light (left) and UV light (right) illumination. c) TEM image of carboxyl-functionalized PBdots. d) Gel electrophoresis of functionalized and bioconjugated PBdots in a 0.7% agarose gel.

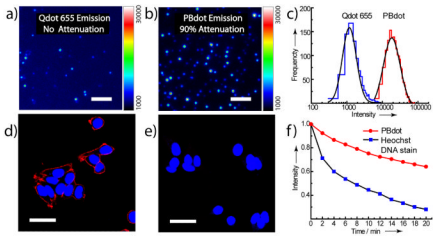

Figure 2.

a) Single-particle image of Qdot 655. b) Single-particle image of PBdots. Both images a) and b) were obtained under identical conditions but 90% of the emitted light from the PBdots was blocked by a neutral density filter (OD=1) to avoid detector saturation. Scale bar, 4 μm. c) Intensity distributions of single-particle fluorescence, showing PBdots are ~15 brighter than Qdot 655 probes. d) Confocal imaging of live MCF-7 cells incubated sequentially with anti-EpCAM primary antibody, biotinylated goat anti-mouse IgG secondary antibody, and PBdot-streptavidin conjugates. Red fluorescence was from PBdots and blue fluorescence was from the nuclear stain Hoechst 34580. Scale bar, 40 μm. e) Negative control for PBdot cell labeling where biotinylated secondary antibody was not used. f) Photobleaching curves extracted from confocal fluorescence images obtained under continuous laser scanning for 20 minutes.

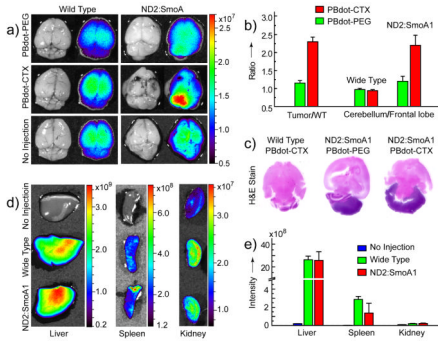

Figure 3.

a) Fluorescence imaging of healthy brains in wild-type mice (left) and medulloblastoma tumors in ND2:SmoA1 mice (right). Each mouse was injected through the tail vein with 50 μL of 1 μM solution of either nontargeting PBdot-PEG (top), or targeting PBdot-CTX (middle). As a control, some mice did not receive injection (bottom). b) Tumor targeting efficiency by quantifying fluorescence signals in ND2:SmoA1 versus wild-type mice and cerebellum versus frontal lobe. c) Histological examination of the mouse brains in a). The dark purple regions in the H&E-stained cerebellum of ND2:SmoA1 mice confirmed the presence of tumor. For comparison, the cerebellum of wild-type mice showed normal cerebellum pathology. d) Biophotonic images of resected livers, spleens, and kidneys from wild-type and ND2:SmoA1 mice receiving Pbdot-CTX injection. e) Biodistribution of the PBdot probes in the resected organs. The biophotonic Images a) and d) were acquired at 72 hours post-injection. The color gradient bar corresponds to the fluorescence intensity (p/s/cm^2/sr) of the images. Each data point in b) and e) is the mean ± s.d. from n=3 animals.